Computation of Spheroidal Micro-organisms Cross Sections Using the Aperiodic Fourier Modal Method

M. Abboud[1, 2], **G. Granet**[1, 2], **K. Edee**[1, 2], **J. F. Cornet**[1, 2], **and J. Dauchet**[1, 2]

[1]Clermont Université, Université Blaise Pascal, BP 10488, F-63000 Clermont Ferrand, France
[2]CNRS, UMR 6602, IP, Aubière F-63177, France

Abstract— In this paper, we investigate the light scattering properties by a spheroidal particle by using the Fourier Modal Method (FMM) equipped with the Perfectly Matched Layers (PMLs). A program which allows the computation of the scattering cross sections and efficiencies has been implemented and checked by comparing the results with those obtained in literature. The effectiveness of the PMLs appeared by plotting the field maps: the interferences from neighbouring periods in the FMM disappeared.

1. INTRODUCTION

Nowadays, our society is facing numerous ecological challenges. Cultivation of photosynthetic micro-organisms within controlled environments such as photobioreactor processes is recognized as a serious alternative to contribute to the CO_2 capture and to produce bio-diesel and bio-hydrogen. In order to optimize conversion of light energy into chemical energy within the process of photosynthesis, we have to predict the light scattering properties, such as the absorption, scattering and extinction cross sections as well as the scattering diagrams [2]. Based on the rigorous solution of Maxwell's equations, Lord Rayleigh [3] and Wait [4] introduced respectively the first formalisms to describe the interaction of a monochromatic plane wave with an isolated infinitely long circular cylinder at normal incidence and oblique incidence. In 1908, Mie [5, 6] derived the exact solution for an homogeneous spherical particle for a very wide range of parameter values. This theory is involved in several applications, e.g., in photobioreactor processes, in environmental monitoring and so on. However, most micro-organisms are not spherical and differ by their size and shape parameters. Their scattering properties are significantly different from those of spherical scatterers. Since it is much more difficult to obtain the exact solution when the scatterer loose the spherical symmetry, a number of approximations have been made in order to calculate the light scattering and absorption properties of non-spherical particles. Among the most prevalent approximations are Waterman's extended boundary condition method also called T-matrix method [7, 8], the finite-difference time-domain method (FDTD) [9] and the finite-element method (FEM) [10]. Asano and Yamamoto [11] obtained solutions for homogeneous prolate and oblate spheroidal particles by solving Maxwell's equations in the spheroidal coordinate system. The main disadvantage of this method is that the vector spheroidal wave functions are not easily calculated, especially for complex arguments that occur with absorbing particles. Nevertheless, a number of numerical results are available. Asano [1] has calculated the scattering and absorption efficiencies and the angular scattering for oriented prolate and oblate spheroids. He obtained results for particles with size parameters up to 30 and axial ratios up to 5. Most of the results are for $m = 1.33$ and $m = 1.5$ although some calculations have been made for absorbing particles with $m = 1.5 + 0.1i$.

In this paper, the Fourier Modal Method is extended to non periodic structure. This is achieved by introducing the perfectly matched layers (PMLs) concept. The remainder of the paper is organized as follows: Section 1 is devoted to the statement of the problem and the derivation of the eigenvalue equation. In Section 2, we present numerical results that are successfully compared with those obtained by Asano.

2. STATEMENT OF THE PROBLEM

Let us consider an arbitrarly particle illuminated by a monochromatic plane wave with angular frequency ω, refractive index ν_1 and wave vector $\mathbf{k}$ which components are:

$$\mathbf{k}\begin{cases} \alpha_0 = k\nu_1 \sin\xi\cos\phi \\ \beta_0 = k\nu_1 \sin\xi\sin\phi \\ \gamma_0 = k\nu_1\cos\xi \end{cases} . \tag{1}$$

The amplitudes of the electric field components of the incident wave are:

$$\left[\begin{array}{c} E_x^{inc} \\ E_y^{inc} \\ E_z^{inc} \end{array}\right] = \left[\begin{array}{ccc} \sin\xi\cos\phi & \cos\xi\cos\phi & -\sin\phi \\ \sin\xi\sin\phi & \cos\xi\sin\phi & \cos\phi \\ \cos\phi & -\sin\xi & 0 \end{array}\right] \left[\begin{array}{c} 0 \\ \cos\delta \\ \sin\delta \end{array}\right], \tag{2}$$

where ξ is the incidence angle, ϕ the azimuthal angle and δ the angle of polarization. The particle is approximated by a staircase profile so that it is replaced by a stack of n_{sl} layers, each of them is characterized by its thickness and its relative permittivity function $\varepsilon(x, y)$. See Figures 1(a) and (b).

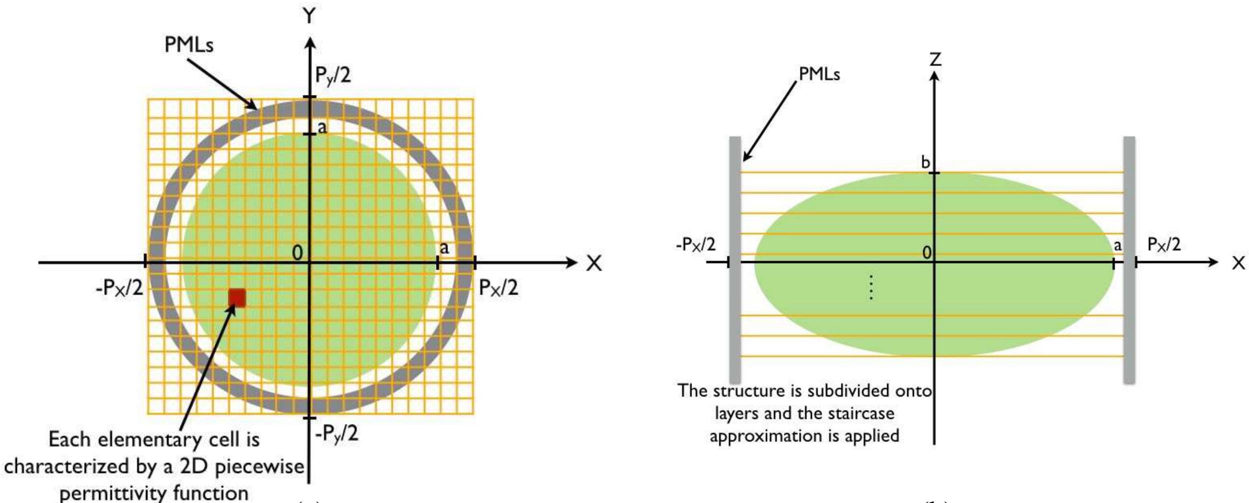

(a) (b)

Figure 1: Configuration of the structure under study.

It can be shown that any component of electromagnetic field can be written as $\Phi(x, y)exp(-ik\gamma z)$, where $k = \omega\sqrt{\varepsilon_0\mu_0}$. ε_0 and μ_0 are the permittivity and the permeability of the vacuum. The numerical process consists in searching a numerical approximation of the functions Φ for all components of the electromagnetic field by imposing boundary conditions. By eliminating the longitudinal components E_z and H_z from Maxwell's equations, we arrive to matrix relations (3) and (4) between transversal components E_x, E_y, H_x and H_y:

$$\boldsymbol{\partial}_z \left[\begin{array}{c} \mathbf{E}_x \\ \mathbf{E}_y \end{array}\right] = \left[\begin{array}{cc} \frac{i}{k}\boldsymbol{\partial}_x\boldsymbol{\mathcal{E}}^{-1}\boldsymbol{\partial}_y & -\frac{i}{k}\boldsymbol{\partial}_x\boldsymbol{\mathcal{E}}^{-1}\boldsymbol{\partial}_x - ik \\ \frac{i}{k}\boldsymbol{\partial}_y\boldsymbol{\mathcal{E}}^{-1}\boldsymbol{\partial}_y + ik & -\frac{i}{k}\boldsymbol{\partial}_y\boldsymbol{\mathcal{E}}^{-1}\boldsymbol{\partial}_x \end{array}\right] \left[\begin{array}{c} H_x \\ H_y \end{array}\right] \tag{3}$$

and

$$\boldsymbol{\partial}_z \left[\begin{array}{c} \mathbf{H}_x \\ \mathbf{H}_y \end{array}\right] = \left[\begin{array}{cc} -\frac{i}{k}\boldsymbol{\partial}_x\boldsymbol{\partial}_y & \frac{i}{k}\boldsymbol{\partial}_x\boldsymbol{\partial}_x + ik\boldsymbol{\mathcal{E}} \\ -\frac{i}{k}\boldsymbol{\partial}_y\boldsymbol{\partial}_y - ik\boldsymbol{\mathcal{E}} & \frac{i}{k}\boldsymbol{\partial}_y\boldsymbol{\partial}_x \end{array}\right] \left[\begin{array}{c} E_x \\ E_y \end{array}\right]. \tag{4}$$

From these equations we can introduce a second order eigenvalue matrix relation:

$$\left\{\begin{array}{l} \boldsymbol{\partial}_z^2 \left[\begin{array}{c} \mathbf{E}_x \\ \mathbf{E}_y \end{array}\right] = \boldsymbol{\mathcal{L}}_{EH}\boldsymbol{\mathcal{L}}_{HE} \left[\begin{array}{c} \mathbf{E}_x \\ \mathbf{E}_y \end{array}\right] \\ \text{or} \\ \boldsymbol{\partial}_z^2 \left[\begin{array}{c} \mathbf{H}_x \\ \mathbf{H}_y \end{array}\right] = \boldsymbol{\mathcal{L}}_{HE}\boldsymbol{\mathcal{L}}_{EH} \left[\begin{array}{c} \mathbf{H}_x \\ \mathbf{H}_y \end{array}\right] \end{array}\right., \tag{5}$$

with

$$\left\{\begin{array}{l} \boldsymbol{\mathcal{L}}_{EH} = \dfrac{1}{k^2}\left[\begin{array}{cc} -\boldsymbol{\partial}_x\boldsymbol{\mathcal{E}}^{-1}\boldsymbol{\partial}_y & \boldsymbol{\partial}_x\boldsymbol{\mathcal{E}}^{-1}\boldsymbol{\partial}_x + k^2\boldsymbol{\mu} \\ -\boldsymbol{\partial}_y\boldsymbol{\mathcal{E}}^{-1}\boldsymbol{\partial}_x - k^2\boldsymbol{\mu} & \boldsymbol{\partial}_y\boldsymbol{\partial}_x \end{array}\right] \\ \boldsymbol{\mathcal{L}}_{HE} = \dfrac{1}{k^2}\left[\begin{array}{cc} -\boldsymbol{\partial}_x\boldsymbol{\mu}^{-1}\boldsymbol{\partial}_y & \boldsymbol{\partial}_x\boldsymbol{\mu}^{-1}\boldsymbol{\partial}_y + k^2\boldsymbol{\mathcal{E}} \\ -\boldsymbol{\partial}_y\boldsymbol{\mu}^{-1}\boldsymbol{\partial}_y - k^2\boldsymbol{\mathcal{E}} & \boldsymbol{\partial}_y\boldsymbol{\partial}_x \end{array}\right] \end{array}\right.. \tag{6}$$

In each layer denoted by the superscript j, one of the eigenvalue equation of Eq. (6) is solved. For example, if the electric eigenvalue equation is solved, the electrical field is written as linear combination of the eigenvectors $[\mathbf{\Phi}_{pq}^j, \mathbf{\Psi}_{pq}^j]^T$ associated to the eigenvalue γ_{pq}:

$$\left\{ \begin{array}{l} |E_x^j\rangle = \sum_{p,q=1}^{2M+1} A_{pq}^j |\mathbf{\Phi}_{pq}\rangle \\ |E_y^j\rangle = \sum_{p,q=1}^{2M+1} A_{pq}^j |\mathbf{\Psi}_{pq}\rangle \end{array} \right. . \tag{7}$$

Each eigenvector $|\mathbf{\Phi}_{pq}\rangle$ and $|\mathbf{\Psi}_{pq}\rangle$ are expanded on finite set of $(2M+1)\times(2M+1)$ Fourier basis functions. Hence, an artificial periodization P_x (resp. P_y) in x-direction (resp. y-direction) is introduced. In order to avoid the effect of this periodization, we introduce PMLs by using complex coordinates transformations in x and y directions [13, 14]. The unknown coefficients A_{pq}^j are calculated through the S matrix propagation algorithm and the reflected R_{pq} and transmitted T_{pq} efficiencies are deduced.

3. NUMERICAL RESULTS

Firstly for a sake of comparison with [1], we consider the following two examples: prolate spheroids with a refractive index $\nu = 1.5$ and oblate ones with $\nu = 1.33$. Recall that a prolate spheroid has one major semi-axis a and two equal minor semi-axes b. An oblate spheroid is characterized by two equal major semi-axes a and one minor semi-axis b. Other variables characterizing these spheroids are: the shape factor a/b and the size parameter $\alpha = 2\pi a/\lambda$. Numerical computations are performed on the spheroids of the size parameters up to 30 and for various values of the shape parameters a/b that fluctuated between 1.5 and 5.

It is of common use to normalize the cross-sections C_{sca} of a spheroid by the area of a sphere having the same volume, $C_{sca}/\pi r^2$ where $r = (a^2b)^{1/3}$ for the oblate spheroid and $r = (ab^2)^{1/3}$ for the prolate spheroid.

Numerical investigations show that results stabilize as soon as the truncation order M reaches 12 and number of layers $n_{sl} = 80$. These results are obtained for an optimized values of $P_x = P_y = 8.33r$. The scattering efficiency factors Q_{sca} are connected with their corresponding cross-sections by this relation:

$$Q_{sca} = C_{sca}/G(\xi). \tag{8}$$

$G(\xi)$ is the area of the particle shadow also called the 'viewing' geometrical cross-section. It depends on the angle of incidence ξ. The geometrical cross section of the prolate spheroid is:

$$G(\xi) = \pi a(b^2 \sin^2\xi + a^2 \cos^2\xi)^{1/2} \tag{9}$$

and of the oblate spheroid is:

$$G(\xi) = \pi b(a^2 \sin^2\xi + b^2 \cos^2\xi)^{1/2}. \tag{10}$$

In Figures 2(a) and (b), the scattering cross sections of oblate and prolate spheroids are plotted at normal incidence ($\xi = 0°$) with respect to the size parameter of the sphere $2\pi r/\lambda$ for different values of a/b. Those results are successfully compared with Figures 4 and 6 of Reference [1].

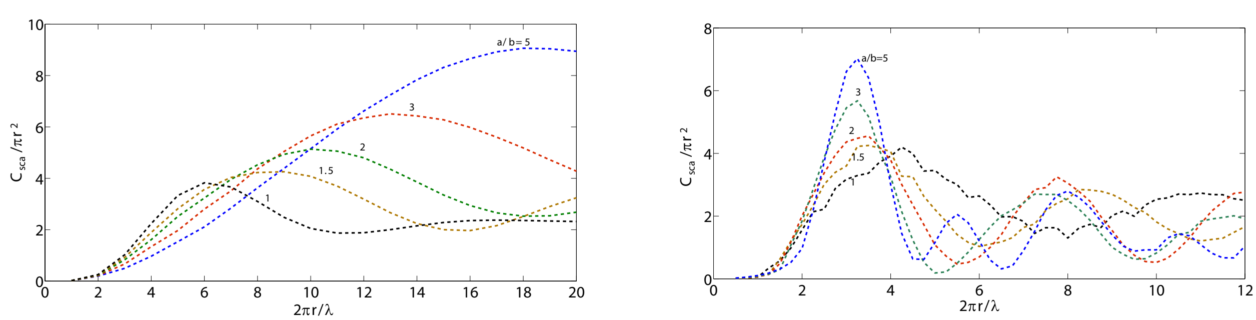

(a) (b)

Figure 2: Scattering cross sections of particles with different ratios. (a) Oblate spheroids, (b) prolate spheroids.

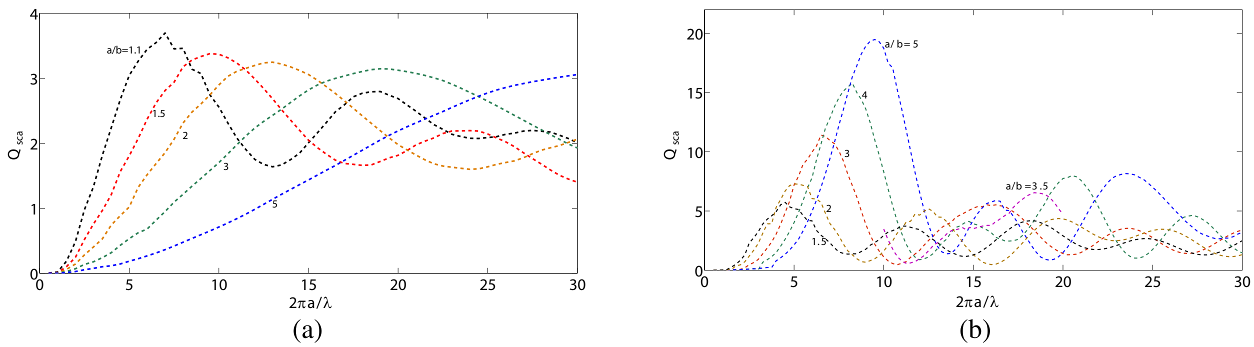

Figure 3: Scattering efficiency of particles with different ratios. (a) Oblate spheroids, (b) prolate spheroids.

Figures 3(a) and (b) show the scattering efficiency factors for the oblate and prolate spheroids at $\xi = 0°$ as a function of the size parameter α for various values of the shape parameters a/b. Asano has obtained the same results in Figures 3 and 5 of Reference [1].

In Figures 4(a) and (b), the scattering efficiency factors of oblate spheroid ($a/b = 3$) and prolate spheroid ($a/b = 5$) are replotted against the size parameter α for three incidence angles $\xi = 0°$, $45°$, and $90°$. In the case of oblique incidence ($\xi \neq 0$), the TE and TM polarizations are involved. Corresponding results are given in figures 7 and 8 in Reference [1].

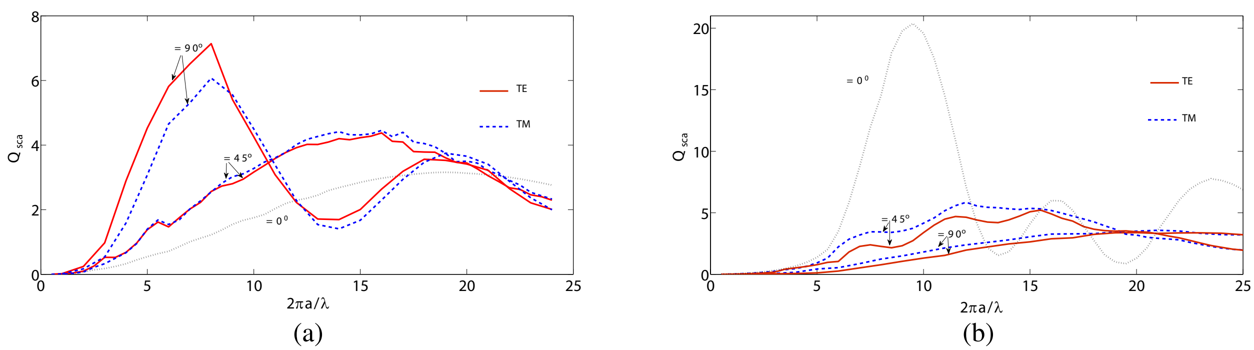

Figure 4: Scattering efficiency of particles with various angle of incidence. (a) Oblate spheroids, (b) prolate spheroids.

Secondly, to show the effectiveness of the Perfectly Matched Layers (PMLs), we compare in Figure 5 the amplitude of the transmitted electric field $\mathbf{E_y}$ computed with and without PMLs of a prolate spheroid for the following numerical parameters: $\lambda = 16.67\,\text{mm}$, $P_x = P_y = 8.33\lambda$, $\nu = 1.2$, $a = 84\,\text{mm}$ and $b = 17\,\text{mm}$. It can be seen that, the neighbouring periods see each others and spurious interferences take place. The comparison of these results emphasizes that the field calculated with the PMLs should be valid, since the parasitic oscillations have disappeared.

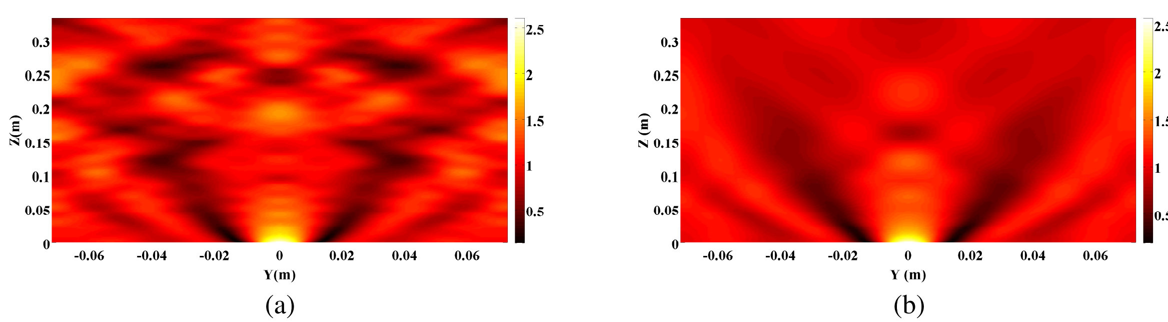

Figure 5: Field map of a prolate spheroid. (a) Without PMLs, (b) with PMLs.

4. CONCLUSION

In this paper, we applied the FMM and the staircase approximation in order to compute the light scattering by spheroidal micro-organism. To avoid the parasitic couplings introduced by the periodizations, the classical FMM is equipped with PMLs through complex coordinates concept. The scattering cross sections and the efficiencies calculated by using this method were successfully compared with results in the literature. To show the crucial role played by the PMLs, a field map, with and without using the PMLs, is presented and satisfactory results are obtained. However, the convergence of the results depends on the number of slices n_{sl} in the staircase approximation but also on the number of eigenfunctions M used to describe the field in each layer. Even though this point is not explicitly detailed in this article, the results reflect a systematic study of their convergence.

ACKNOWLEDGMENT

This work was funded by grants from the *European Comission* (Auvergne FEDER funds) and the *Region Auvergne* in the framework of the LabEx IMoBS3.

REFERENCES

1. Asano, S., "Light scattering properties of spheroidal particles," *Appl. Opt.*, Vol. 18, No. 5, 712–723, 1979.
2. Cornet, J.-F., "Calculation of optimal design and ideal productivities of volumetrically lightened photobioreactors using the constructal approach," *Chem. Eng. Sci.*, Vol. 65, No. 2, 985–998, 2010.
3. Rayleigh, L., "On the problem of random vibrations, and of random flights in one, two, or three dimension," *Phil. Mag.*, Vol. 37, No. 6, 321–347, 1919.
4. Wait, J. R., "Scattering of a plane wave from a circular dielectric cylinder at oblique incidence," *Can. J. Phys.*, Vol. 33, No. 5, 189–195, 1955.
5. Van de Hulst, H. C., *Light Scattering by Small Particles*, Dover Publication Inc., New York, 1981.
6. Bohren, C. F. and D. R. Huffman, *Absorption and Scattering of Light by Small Particles*, Wiley-Interscience, New York, 1983.
7. Waterman, P. C., "Matrix formulation of electromagnetic scattering," *Proc. IEEE*, Vol. 53, No. 8, 805–812, 1965.
8. Waterman, P. C., "Symmetry, unitarity, and geometry in electromagnetic scattering," *Phys. Rev.*, Vol. D, No. 3, 825–839, 1971.
9. Prather, D. W. and S. Shi, "Formulation and application of the finite-difference time-domain method for the analysis of axially symmetric diffractive optical elements," *J. Opt. Soc. Am.*, Vol. A, No. 16, 1131–1142, 1999.
10. Morgan, M. A. and K. K. Mei, "Finite element computation of scattering by inhomogeneous penetrable bodies of revolution," *IEEE Trans. Antennas Propagat.*, Vol. AP, No. 27, 202–214, 1979.
11. Asano, S. and G. Yamamoto, "Light scattering by spheroidal particles," *Appl. Opt.*, Vol. 14, No. 14, 29–49, 1986.
12. Asano, S. and M. Sato, "Light scattering by randomly oriented spheroidal particles," *Appl. Opt.*, Vol. 19, No. 6, 962–974, 1980.
13. Edee, K. and B. Guizal, "Modal method based on subsectional Gegenbauer polynomial expansion for nonperiodic structures: Complex coordinates implementation," *JOSA A*, Vol. 30, No. 4, 631–639, 2013.
14. Edee, K. ,G. Granet, and J. P. Plumey, "Complex coordinate implementation in the curvilinear coordinate method: Application to plane-wave diffraction by nonperiodic rough surfaces," *JOSA A*, Vol. 24, No. 4, 1097–1102, 2007.